POLITECNICO DI TORINO
Repository ISTITUZIONALE

Parametric study of the radiative load distribution on the EU-DEMO first wall due to SPI-mitigated disruptions

Original
Parametric study of the radiative load distribution on the EU-DEMO first wall due to SPI-mitigated disruptions / Moscheni, M.; Carr, M.; Dulla, S.; Maviglia, F.; Meakins, A.; Nallo, G. F.; Subba, F.; Zanino, R.. - In: FUSION ENGINEERING AND DESIGN. - ISSN 0920-3796. - ELETTRONICO. - 172:(2021), p. 112917. [10.1016/j.fusengdes.2021.112917]

Availability:
This version is available at: 11583/2938772 since: 2021-11-19T01:17:54Z

Publisher:
Elsevier Ltd

Published
DOI:10.1016/j.fusengdes.2021.112917

Terms of use:

This article is made available under terms and conditions as specified in the corresponding bibliographic description in the repository

Publisher copyright
Elsevier postprint/Author's Accepted Manuscript

© 2021. This manuscript version is made available under the CC-BY-NC-ND 4.0 license http://creativecommons.org/licenses/by-nc-nd/4.0/.The final authenticated version is available online at: http://dx.doi.org/10.1016/j.fusengdes.2021.112917

(Article begins on next page)

09 May 2024

Parametric Study of the Radiative Load Distribution on the EU-DEMO First Wall Due to SPI-Mitigated Disruptions

M. Moscheni[(1)], M. Carr[(2)], S. Dulla[(1)], F. Maviglia[(3)], A. Meakins[(2)], G.F. Nallo[(1)], F. Subba[(1)], and R. Zanino[(1)]

[(1)] *NEMO Group, Dipartimento Energia, Politecnico di Torino, Corso Duca degli Abruzzi 24, 10129, Torino, Italy*
[(2)] *Luffy AI, Culham Science Centre, Abingdon, OX14 3DB, United Kingdom*
[(3)] *EUROFusion PMU, Boltzmannstrasse 2, Garching bei Munchen, Germany*

Plasma disruptions are rapid and dramatic off-normal operation events, lasting only a few milliseconds, which can damage the tokamak in-vessel structures. Shattered Pellet Injection (SPI) can be employed to mitigate these transients. This technique consists of injecting impurities to enhance the isotropic radiation emission, thus reducing the peak heat load onto the Plasma Facing Components (PFCs). In this work, we employ the CHERAB code to assess the radiative heat load on the EU-DEMO in-vessel structures following a disruption mitigated via SPI with 0.5 GJ of radiated energy. The effect of different penetration depths of shattered pellets varying in the range 0.2-3.5 m is parametrically studied. The computed peak radiative load in the case of deep deposition of the impurities ($\sim 5.6 \cdot 10^2$ MW/m^2) is around 18 times smaller than in the case of shallow penetration ($\sim 1.0 \cdot 10^4$ MW/m^2). Instead, a figure for an intermediate penetration would be $\sim 1.5 \cdot 10^3$ MW/m^2.

Keywords: EU-DEMO, plasma disruptions, shattered pellet injection, first wall radiative load

1. Introduction

Plasma disruptions are dramatic off-normal operation events, lasting only a few milliseconds [1] and involving the sudden loss of plasma confinement, which can result in extensive damages of tokamak in-vessel structures. The EU-DEMO First Wall (FW), armoured with a 2-mm-thick W coating [2] [3], is of particular concern as it is relatively less resilient to plasma transients than the ITER FW [4] [5] due to the harsh neutron fluence environment in which it will operate. Therefore, if the control system detects the precursors of an upcoming disruption, Massive Gas Injection (MGI) or Shattered Pellet Injection (SPI) can be employed as mitigation strategies [6] [7]. Impurity injection aims at enhancing the isotropic radiation emission to spread the plasma energy as uniformly as possible onto the Plasma Facing Components (PFCs), consequently reducing the peak heat load. Among other parameters, the mitigation efficiency strongly depends on where the impurities are deposited in the plasma. Therefore, although the mitigation system is triggered, it is not granted that the resulting mitigated load on the structures would be lowered down to an acceptable level, as also suggested by our previous study [8]. In this respect, SPI appears more promising than MGI, as it is characterized by a faster and deeper penetration, and consequently by a larger core radiation emission [9] [10].
In this work, the Monte Carlo (MC) ray-tracing code CHERAB [11] [12] [13] is employed to assess the radiative heat load distribution on the EU-DEMO FW following a SPI-mitigated disruption (MD) with 0.5 GJ of radiated energy. As the actual penetration depth of shattered pellets is affected by significant uncertainties [1] [14], we perform a parametric study considering three realistic radiation sources corresponding to increasing penetration depths. For comparison, we also perform calculations of radiative heat loads during normal operation (from Start Of Flat-top, SOF, to End Of Flat-top, EOF) for which a careful *ad hoc* quality assurance procedure is required.
The paper is organized as follows: in Sec. 2 we describe the methodology and quality assurance; in Sec. 3, we present and discuss the results in the two different scenarios of off-normal and normal operation); in Sec. 4 we list conclusions and perspectives of this work.

2. Methodology

2.1. Simulation setup

2.1.1. Input: computational meshes

Due to data availability reasons in the constantly-evolving framework of the pre-conceptual design phase, calculations for the off-normal (MD) and normal (SOF/EOF) operation scenarios are performed using two slightly different CAD models of the EU-DEMO FW, shown in Fig. 1. These models are respectively divided into 150 [15] and 89 [16] sub-pieces and they mainly differ in terms of location of the LIMiters (LIMs, Fig. 1). On each sub-piece, an unstructured triangulation is defined, which represents the computational mesh of the simulation [8]. The small average triangle linear size ($\lesssim$ 1 cm), together with suitable local refinements (Fig. 1), ensure a satisfactory space resolution of the computed load distribution [8] [17].
For toroidally symmetric sources (Sec. 2.1.2) and according to the periodicities of the PFCs along the toroidal direction φ [rad] [15], the computational domain could be reduced to 1/4 of the tokamak. Nevertheless, to lower the computational time, we perform our calculations over one or two (depending on the considered source) reference sectors, A and B, (1/16 of the EU-DEMO chamber each) equipped with all LIMs (Fig. 1 for Sector A). This choice is acceptable since the limiters are the PFCs of most concern, as they protrude out of the wall towards the source.

Corresponding author's email: giuseppefrancesco.nallo@polito.it

As it is evident from Fig. 1, the sub-pieces of the SOF/EOF mesh are separated by relatively small gaps. Their presence has to be taken into account when assessing the overall energy conservation of the simulation.
In the current work, the surface of the whole sector included in the simulations is assumed to be a perfect radiation absorber [6] [8]. Indeed, we expect that modelling or not reflection would be of little relevance for what concerns the radiative load on the FW and limiters. Furthermore, taking reflection into account is possible in CHERAB, but it would introduce significant complexity and require further information about material properties, e.g., the dependence of the reflection index on the wavelength of the incident radiation, on the surface roughness and on the degree of transmutation of the material [18]. Nonetheless, rays repeatedly reflected by the walls can be channeled in the DIV region actually giving an increase in the radiative load computed there [19], which should however be of little concern thanks to the heat handling capability of the divertor targets. Studies to quantify the importance of this effect are planned for the future.

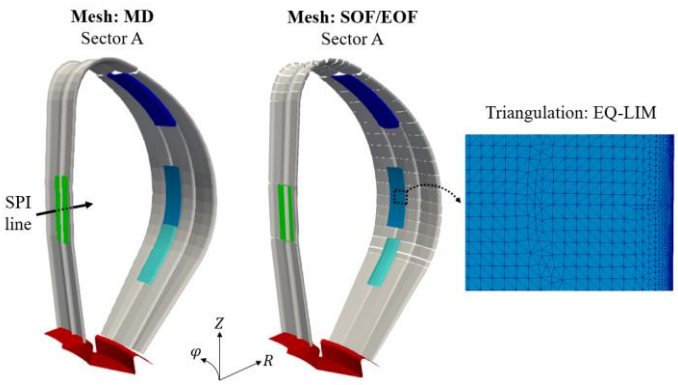

Figure 1. Geometry of the EU-DEMO reference sectors (Sector A, $\Delta\varphi_A = (-\pi/16\,;\,+\pi/16)$) adopted to compute the radiative heat load from MD (left) – with IMP SPI line – and SOF/EOF (right). Both geometries are provided with four limiters: inner (IN-LIM), upper (UP-LIM), equatorial (EQ-LIM) and lower (LOW-LIM). The zoom over EQ-LIM shows the unstructured triangulation characterized by localized refinements.

2.1.2. Input: radiation sources

In the present work, we consider radiation sources associated to both MD and SOF/EOF scenarios. For both cases, we neglect any anisotropy, as well as any wavelength or time dependence in the radiation emission [8]. The main features of the sources are described in the following.

i. MD scenario. The effect of varying the penetration depth (measured from IMP, $\varphi_{\mathrm{SPI}} = 0$) of the injected shattered pellet is explored, as this quantity is affected by significant uncertainties [1] [14]. It is noteworthy underlying that this paper does not deal with a design of the SPI system, which was not available in the pre-conceptual design of DEMO. The location of these radiation sources is meant to be used to develop and test the CHERAB code. It appears highly improbable that a SPI system shooting pellets from the IMP could be technologically viable.
Three different situations are considered in this parametric study (see Tab. 1, first column):

- Shallow (1) and intermediate (2) penetration, where the injected impurities are assumed to travel along R for 0.2 m and 1.8 m inside the plasma (from IMP), respectively, before being ablated and starting to flow along the helicoidal magnetic field lines. It is assumed that 50% of the impurities are directed towards $\varphi > 0$ and 50% towards $\varphi < 0$. Consistently with experimentally measured toroidal transit times [20], the resulting radiation emission distribution is assumed to be a 3D helix spanning one single toroidal revolution, $\Delta\varphi = (-\pi\,;\,+\pi)$ [21], whose circular projections on the poloidal plane (having radii $r_1 = 2.9$ m and $r_2 = 1.7$ m, respectively) are pictured in Tab. 1 (first column, first and second row). From these pictures, the choice of the two penetration depths considered can be explained: r_1 is the maximum radius which allows source 1 to fit in in the DEMO chamber, while r_2 is such that the poloidal projection of source 2 is centered in the plasma axis and lies within the projection of source 1.
The number of poloidal revolutions $n_1 = 1/6$ and $n_2 = 1$ completed during the one toroidal revolution is dictated by the assumed safety factors $q_1 = 6$ (conservatively at the plasma periphery) and $q_2 = 1$ (in the core plasma) via $n = 1/q$ [22]. With $n_1 < 1$, the circular projection for source 1 is travelled only partially (solid line in Tab. 1, first column, first row).

For both source 1 and source 2, we simulate two identical, diametrically opposed sectors (Fig. 1, left), Sector A, with $\Delta\varphi_A = (-\pi/16\,;\,+\pi/16)$, and Sector B, for which $\Delta\varphi_B = \Delta\varphi_A + \pi$, to capture the most relevant features of the heat load distribution (e.g. its maximum and minimum) while avoiding an unnecessary increase of the computational time.

- Deep (3) penetration, where the injected impurities are assumed to travel along R up to the plasma axis, i.e. 3.4 m in the plasma (from IMP). Since ($q \to +\infty$) on the plasma axis, a toroidally symmetric source ($n_3 = 0$) is assumed. In this case, it is sufficient to simulate Sector A only.

The poloidal cross section of each of the three sources is a square (with side length of 10 cm) which is assumed for the sake of simplicity and does not imply any drawbacks in the ray-tracing procedure [17]. Instead, 10 cm is consistent with cross-field particle diffusion detected in experiments [20].
Also commonly to all the MD sources, we assume a short duration of the event $\tau_{\mathrm{MD}} = 1$ ms [23], to be conservative, and to approximately include a possible temporal peaking of the radiation emission. Then, we compute a corresponding total power radiated $P^*_{\mathrm{tot}} = 500$ GW, uniformly distributed in the source volume [8].

ii. Steady-state (SOF/EOF) scenario. The overall radiation emission distribution, computed on Sector A only, is the result of the superposition of two toroidally symmetric contributions:

- Core plasma. The spatial distribution of the radiation source in the core plasma is computed by means of the ASTRA code [24]. The total power radiated in the core for the scenario considered is $P^*_{\mathrm{Core}} =$ 303.75 MW.
- SOL plasma. This region is modelled via the SOLPS-ITER code by assuming an EU-DEMO-relevant and highly-radiative scenario [25]. Different impurities (noble gases and nitrogen) seeded by means of gas puffing are modelled too. The resulting spatial distribution of the radiation emission has been rescaled by a factor 1.385 to obtain, starting from the 93.863 MW computed by SOLPS-ITER, a total radiated power in the SOL of $P^*_{\mathrm{SOL}} = 130$ MW, in line with more recent estimates [5]. Overall, this scenario is compatible with a safe divertor operation [25].

The SOLPS-ITER computational domain extends radially inside the Last Closed Magnetic Surface (LCMS), to approximately make space for the pedestal region. Therefore, this region is included in both ASTRA and SOLPS-ITER simulations. For the sake of simplicity, only the ASTRA solution is retained inside the LCMS, whereas in the SOL the SOLPS-ITER solution is used [26]. This procedure leads to the overall (Core + SOL) radiative emission map shown in Fig. 2 (right). The total radiated power is therefore $P^*_{\mathrm{tot}} = P^*_{\mathrm{Core}} + P^*_{\mathrm{SOL}} =$ 433.75 MW.
Core and SOL are treated as two distinct sources in CHERAB. This allows adopting different *ad hoc* settings for the ray-tracing procedure in the two different regions (see Sec. 3). The resulting radiative load on each detector and its corresponding uncertainty are then computed as $q_i = q_i^{\mathrm{Core}} + q_i^{\mathrm{SOL}}$ and $\Delta q_i = \sqrt{\left(\Delta q_i^{\mathrm{Core}}\right)^2 + \left(\Delta q_i^{\mathrm{SOL}}\right)^2}$ [27], respectively.

2.2. Ray-tracing: radiative heat load computation

The CHERAB code employs Raysect as a ray-tracing engine [12] [28]. Rays of light are traced from the source (Sec. 2.1.2) to the computational mesh (Sec. 2.1.1) according to a reverse ray-tracing MC technique (Fig. 2). Each one of the N_{tr} triangles in the mesh represents a radiation detector. N_{ray} rays (scanned by the index $k \in [1; N_{\mathrm{ray}}]$) are shot from each detector (scanned by the index $i \in [1; N_{\mathrm{tr}}]$). The kth ray is uniquely identified by an origin (randomly selected over the detector area) and a direction (randomly selected in the half-space in front of the detector). As the kth ray is followed (*traced*), any non-uniform[1] source of radiation [W/m^3/sr] is sampled in space, according to a tunable source-sampling step (SSS) Δs. The 1D integration in space of these samples yields the radiance L_i^k [W/m^2/sr] associated to the kth ray fired by the ith detector. The integration of the N_{ray} radiances over the detector area A_i [m^2] (where origins are distributed) and over the 2π solid angle [sr] (where directions are distributed) then provides the radiative power P_i [W] impinging over the ith detector alongside with the corresponding statistical uncertainty ΔP_i [W]. Eventually, the radiation heat load $q_i = P_i/A_i$ [W/m^2] and its uncertainty $\Delta q_i = \Delta P_i/A_i$ [W/m^2] are computed, from which the corresponding MC uncertainty $\varepsilon_i = \Delta q_i/q_i$ [-] ($q_i \neq 0$) follows. The average relative error ε, obtained as the arithmetic average of the set $\{\varepsilon_i\}$, approximately quantifies the overall precision of the simulation [8]. The total power P_{tot} [W] reaching the entire computational mesh and its absolute uncertainty ΔP_{tot} [W] [27] can be evaluated and compared with the expected output P^*_{tot} to assess the energy conservation.

[1] e.g. SOF/EOF source. MD source is uniform and, therefore, L_i^k are trivially evaluated by multiplying the source strength and the distance between the first and the last intersection of the ray with the source itself (respectively, the entrance and the exit point computed by the ray-tracing engine).

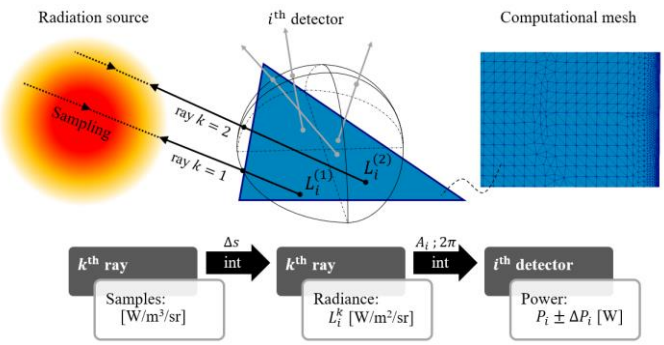

Figure 2. Power calculation scheme. Each triangle in the mesh becomes a detector firing N_{ray} rays. Samples of a non-uniform radiation source are acquired for the kth ray according to a suitable source-sampling step Δs and integrated to get the radiance L_i^k. The radiance samples are, in turn, integrated over the area A_i of the detector and over the 2π solid angle to retrieve the power P_i (and the corresponding uncertainty) on the ith detector.

2.3. Simulation quality assurance

2.3.1. Source-sampling step independence

The source-sampling step Δs, defined in Sec. 2.2, must be sufficiently small with respect to the characteristic length of the gradients of the radiation source. If this condition is not met, regardless of the chosen value of N_{ray}, the source gradients may not be correctly resolved, thereby resulting in a lack of accuracy (quantified by the relative variation with respect to the exact value [8] [17]) of q_i. Therefore, an SSS independence study (not reported here) has been performed to suitably tune the step for the SOF/EOF source.

2.3.2. Energy conservation

In the present work, the mesh triangles are detectors shooting rays from their surface (see Sec. 2.2) and perfect absorbers of rays (see Sec. 2.1.1) at the same time. Therefore, self-absorption of rays (ray trapping [17]) is avoided from the very beginning by shifting the detector away from the mesh triangle by $\delta\varrho \sim 1$ mm in the direction of the source. If such a procedure is not carried out, self-absorption would cause a loss of precision (i.e. increase of ε_i) and accuracy on q_i.
On the other hand, given that the surface A_i of the detector is left unchanged, the shortening of the source-detector distance ϱ results in an overestimation of q_i by a factor in the order of[2] $\sim 2 \cdot (\delta\varrho/\varrho)$ [17]. Although the error introduced in each q_i is typically negligible, the building up of tiny overestimations affects the computation of the total power detected [17], and hence must be taken into account when discussing energy conservation.
Unfortunately, as per MD source 1 and 2, the lack of toroidal symmetry accompanied by the simulation of only a fraction of the tokamak lead to the impossibility of checking for the energy conservation (Tab. 3).

3. Results and discussion

The leading input parameters and the resulting radiative heat load distribution for each MD and SOF/EOF simulation are listed in Tab. 1 and 2, respectively. Common characteristics of the different simulations are [8]: (i) the application of the averaging procedure (AVG) to smooth out the Monte Carlo statistical fluctuation; (ii) the adoption of a sufficiently large number of rays per detector N_{ray} to allow for a precise evaluation of the peak radiative load. Further scenario-specific discussions are held in the following.
The dataset containing the full simulation input and output for both the MD and the SOF/EOF case is available at [29]. This includes scripts for simulation pre- and post- processing.

[2] For what concerns a distributed non-uniform source (e.g. SOF/EOF), work is still ongoing, although the practical experience suggests that the overestimation is of minor importance.

Table 1. SPI-mitigated disruption scenario (MD). From left to right: sources of radiation (poloidal plane), enlarged for the sake of a better visualization; leading input parameters; resulting radiative heat load on Sector A and B (except for source MD-3), inboard and outboard.

Source	Input parameters	Sector A		Sector B	
		Inboard	Outboard	Inboard	Outboard
MD-1 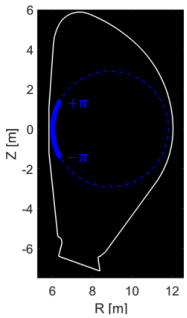	Number of rays: $N_{\mathrm{ray}} = 10000$ Integration step: $\Delta s = -$ Offset: $\Delta\varrho = 1\text{e-}6$ m	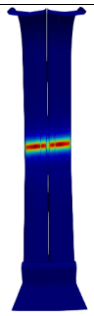		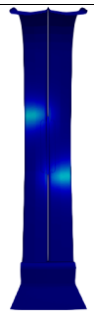	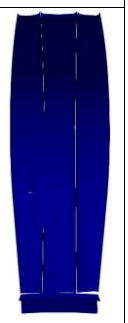
		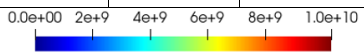			$\langle q \rangle$ [W/m^2]
MD-2 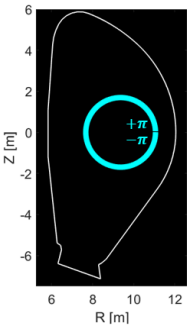	Number of rays: $N_{\mathrm{ray}} = 10000$ Integration step: $\Delta s = -$ Offset: $\Delta\varrho = 1\text{e-}3$ m	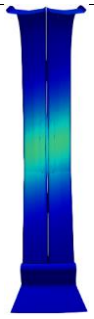			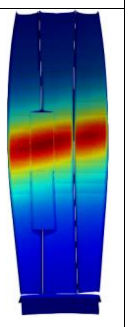
		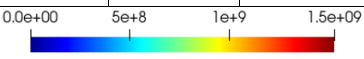			$\langle q \rangle$ [W/m^2]
MD-3 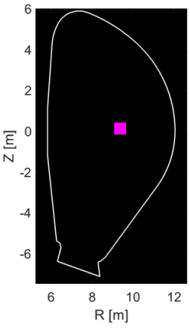	Number of rays: $N_{\mathrm{ray}} = 10000$ Integration step: $\Delta s = -$ Offset: $\Delta\varrho = 1\text{e-}3$ m	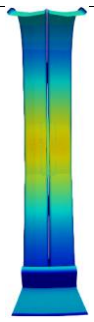	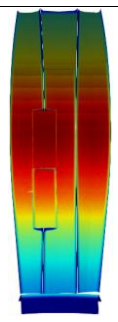	–	–
		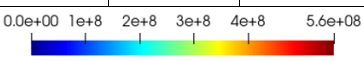			$\langle q \rangle$ [W/m^2]

Table 2. Steady-state scenario (SOF/EOF). From left to right: source of radiation (poloidal plane, log scale), ASTRA data for the core and SOLPS-ITER data for SOL plasma; leading input parameters; resulting radiative heat load on Sector A, inboard and outboard, with and without divertor PFCs.

Source	**Input parameters**	**Sector A: FW + LIMs + DIV**		**Sector A: FW + LIMs**	
		Inboard	**Outboard**	**Inboard**	**Outboard**
SOF/EOF: Core + SOL 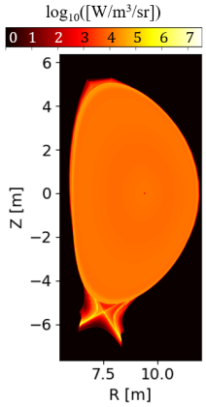	Number of rays: $N_{\mathrm{ray}}^{\mathrm{Core}} = 1000$ $N_{\mathrm{ray}}^{\mathrm{SOL}} = 1500$ Integration step: $\Delta s_{\mathrm{Core}} =$ 1e-2 m $\Delta s_{\mathrm{SOL}} =$ 1e-3 m Offset: $\Delta \varrho =$ 1e-6 m	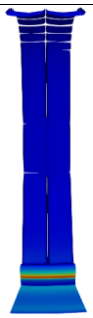			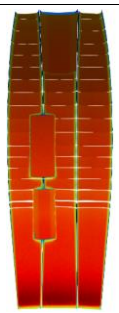
		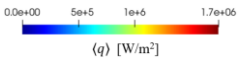		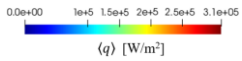	

Table 3. Main outputs of the different simulations. The number of significant digits follow from the corresponding precision. All simulations have been run with OMP parallelism on a 16x2 cores cluster node with Intel® Xeon® Gold Scalable Processor Gold CPU 6130 @2.10 GHz.

Scenario	**Source**	**MC average error ε [%]**	$\boldsymbol{P_{\mathrm{tot}}}$ **vs.** $\boldsymbol{P_{\mathrm{tot}}^{*}}$	$\boldsymbol{q_{\mathrm{max}}}$ **[MW/m²]**	$\boldsymbol{q_{\mathrm{max}}}$ **location**	**CPU time [days]**
MD	1	2.3	- / 500.00 GW	$1.03 \cdot 10^{4}$	IMP FW	9×2
	2	2.0	- / 500.00 GW	$1.52 \cdot 10^{3}$	Outboard EQ-LIM	9×2
	3	1.1	498.96 / 500.00 GW	$5.57 \cdot 10^{2}$	Outboard EQ-LIM	7
SOF/EOF	Core + SOL	0.9	423.20 / 433.75 MW	1.71	Outboard DIV target	80
				0.311	Lower outboard FW, excluding DIV region	

3.1. Mitigated disruption scenario: parametric study

In the MD scenario, the selected $N_{\mathrm{ray}} = 10000$ is 4 times larger than in our previous work [8] to guarantee satisfactory precision and accuracy despite the limited spatial extension of the source [17]. Here, no SSS is involved as the radiation source is uniform in space. As shown in Tab. 1 (second column), the offset $\delta\varrho = 1\ \mu$m adopted for source 1 is 1000 times smaller than in the other MD cases. Indeed, due to the proximity of the source to the IMP computational mesh, the error introduced by shifting the detector 1 mm away from the surface would be non-negligible (up to 2 GW [17]). The resulting radiative heat load distributions in Tab. 1 show that, as expected, a deeper deposition of the impurities determines a more uniform distribution and a lower peak radiative load. Quantitatively, the peak radiative load decreases by a factor of ~ 18 from shallow (source 1, $1.03 \cdot 10^{4}$ MW/m²) to deep (source 3, $5.57 \cdot 10^{2}$ MW/m²) penetration. Nonetheless, source 3 may not be feasible in practical EU-DEMO scenarios due to the strong outward-pointing drift generated by the high temperature of the plasma, which prevents ablated impurities from penetrating [1] [14]. Therefore, the peak radiative load obtained with an intermediate pellet penetration (source 2, $1.52 \cdot 10^{3}$ MW/m²) may be more representative in EU-DEMO perspective.

For what concerns the location of the maximum, while the peak radiative load falls on the IMP FW for the case of source 1 (Sector A), it is attained over outboard EQ-LIM with source 2 (Sector B) and 3 (Sector A).

The restrictive assumptions (common to both MD and SOF/EOF scenarios) of isotropic emission in the source modelling (Sec. 2.1.2) can be softened by multiplying the peak load $q_{\max}$ by a conservative ITER-like peaking factor γ (~ 3 for ITER [5] [16] [30]), i.e. $q_{\max} \rightarrow \gamma \cdot q_{\max}$.
Also, when dealing with transient events, it is common to introduce the peak heat impact factor (PHIF, expressed in J · m^{-2} · s$^{-0.5}$) [5] [10]. This factor is defined as the product of the peak heat load $q_{\max}$ [W/m^2] and the square-root of the duration of the transient τ [s], i.e. PHIF $= (q_{\max} \cdot \sqrt{\tau})$. Such quantity comes from the solution of the 1D heat diffusion equation in a semi-infinite slab subject to a surface heat pulse [31]. This approximation holds here because the thermal quench duration ($\tau_{\mathrm{MD}} = 1$ ms) is much shorter than the heat conduction time into the FW and the resulting Fourier number is well below 0.2 [32]. Comparing the PHIF value with estimated limits ($\sim$ 10 MJ · m^{-2} · s$^{-0.5}$ for W [16] [33]) allows assessing the damage to solid structures.
In the present work, with $\tau = \tau_{\mathrm{MD}}$, the melting of the W layer is reached even in the case of source 3 ($q_{\max} = 5.57 \cdot 10^2$ MW/m^2) and even without accounting for any peaking factor, as the corresponding PHIF reads 17.6 MJ · m^{-2} · s$^{-0.5}$. On the one hand, adding reflection in the modelling should reduce the maximum radiative load, according to what we expect, and it is suggested to likely lower the peaking factor too [6]. Similar consequences would also be foreseen if self-protecting mechanisms like vapor (or plasma) shielding [5] and/or multiple shattered pellet injection [1] [14] are modelled. On the other hand, a more detailed description of the source of radiation often leads to an increase of the calculated loads [5].

3.2. Steady-state scenario

In the SOF/EOF scenario, particular caution is needed concerning the choice of the SSS. In the Core emission map, mild gradients are localized at the boundary of the core region and $\Delta s_{\mathrm{Core}} =$ 1e-2 m is sufficient to obtain a satisfactory resolution of the source. Conversely, we set $\Delta s_{\mathrm{SOL}} =$ 1e-3 m due to the steep gradients in the SOL radiation emission near the separatrix. In the light of Sec. 2.3.1, we successfully verified the independence of the peak radiative heat load from such SSSs by scanning the intervals [1e-2 ; 5e-4] m for Core and [1e-3 ; 1e-4] m for SOL. Moreover, $N_{\mathrm{ray}}^{\mathrm{Core}} = 1000$ while $N_{\mathrm{ray}}^{\mathrm{SOL}} = 1500$ as the SOL radiation emission map is more localized in space as compared to Core.
The missing power indicated in Tab. 3 (423.20 MW detected vs. 433.75 MW radiated) can be carefully motivated in terms of the presence of gaps in the mesh (Sec. 2.1.1). Still, this does not pose any threat to the reliability of the outcome as: (i) the peak radiative load would surely not be attained in the place of any gap; (ii) reflection is not modelled.
The results of the steady-state calculation are shown in Tab. 2. The computed overall (FW + LIMs + DIV) radiative load distribution appears to be significantly peaked over the outboard DIV plate with a maximum of 1.71 MW/m^2. The distribution outside the DIV region (FW + LIMs) is instead characterized by a higher uniformity and a peak load of 0.311 MW/m^2 occurring on the lower outboard FW. Such figures are in qualitative agreement with previous simulations of the EU-DEMO normal operation heat load, performed by means of a different computational tool [5]. Moreover, in either case, the steady-state requirements on the peak ($\lesssim$ 10 MW/m^2 on DIV [25] [34] and $\lesssim$ 1-1.5 MW/m^2 on FW [4] [5] [6]) are fulfilled even by accounting for the peaking factor.

4. Conclusions and perspective

In this work, the CHERAB code was tested by evaluating the radiative heat load distribution over the EU-DEMO PFCs. Wavelength and time dependence of the emitted radiation were neglected, and the source was assumed to be isotropic. For all the simulations performed, energy conservation was checked, as well as the independence of the results on the mesh, N_{ray} and SSS.
First, we presented the results of the simulations related to a scenario of a plasma disruption mitigated by means of SPI. We performed a parametric study changing the pellet penetration depth from the IMP, as this is an uncertain parameter. Although the injection from IMP in EU-DEMO itself is unlikely to be practically implemented, this scenario embodied a suitably challenging testbed for the CHERAB code.
The parametric study showed that the maximum power load $q_{\max}$ is: $\sim 1.0 \cdot 10^4$ MW/m^2 on the inboard FW mid-plane with shallow penetration; $\sim 1.5 \cdot 10^3$ MW/m^2 and $\sim 5.6 \cdot 10^2$ MW/m^2 on the outboard equatorial limiter with, respectively, intermediate and deep penetration. Nevertheless, even in this last, more favorable condition - which is not necessarily feasible in practice - and even neglecting any peaking factor, we estimated that the peak heat impact factor with a deep penetration of the impurities is $\sim$ 18 MJ · m^{-2} · s$^{-0.5}$, which is larger than the W damage threshold of $\sim$ 10 MJ · m^{-2} · s$^{-0.5}$ [16] [33]. Nonetheless, further studies at a higher level of detail to compute more accurate estimates of the peak heat impact factor are planned.
Second, we showed the results of a radiative heat load calculation in normal operation scenario. With a computed maximum heat load of $\sim$ 1.7 MW/m^2 on the outboard DIV plate and $\sim$ 0.31 MW/m^2 on the lower outboard FW segments, steady-state constraints are satisfied even if the peaking factor ($\sim$ 3) is accounted for.
In perspective, we plan to include in our model reflecting solid surfaces, wavelength dependence of the radiation emission [20] and more realistic source geometries. Considering multiple SPI also represents an attractive improvement of the baseline approach here discussed [1].

Acknowledgments

This work has been carried out within the framework of the EUROfusion consortium and has received funding from the Euratom research and training programme 2014-2018 and 2019-2020 under grant agreement No 633053. The views and opinions expressed herein do not necessarily reflect those of the European Commission.
Computational resources were provided by HPC@POLITO, a project of Academic Computing within the Department of Control and Computer Engineering at the Politecnico di Torino (http://www.hpc.polito.it).

References

[1] G. Pautasso, E. Fable, F. Koechl, P. Lang, M. Siccinio and F. Maviglia, "Modelling of Shattered Pellet Ablation: a Discussion," *46th EPS Conference on Plasma Physics*, vol. 3.1, pp. 3-6, 2019.

[2] F. A. Hernandez, P. Pereslavtsev, G. Zhou, H. Neuberger, J. Rey, Q. Kang, L. V. Boccaccini, E. Bubelis, I. Moscato and D. Dongiovanni, "An enhanced, near-term HCPB design as driver blanket for the EU DEMO," *Fusion Engineering and Design*, vol. 146, pp. 1186-1191, 2019.

[3] E. Martelli, A. Del Nevo, P. Arena, G. Bongiovì, G. Caruso, P. A. Di Maio, M. Eboli, G. Mariano, R. Marinari, F. Moro, R. Mozzillo, F. Giannetti, G. Di Gironimo, A. Tarallo, A. Tassone and R. Villari, "Advancements in DEMO WCLL breeding blanket design and integration," *Int. J. Energy Res.*, vol. 42, pp. 27-52, 2018.

[4] F. Cismondi, "Progress in EU Breeding Blanket design and integration," *Fusion Engineering and Design*, vol. 136, pp. 782-792, 2018.

[5] R. Wenninger, R. Albanese, R. Ambrosino, F. Arbeiter, J. Aubert, C. Bachmann, L. Barbato, T. Barrett, M. Beckers e W. Biel, «The DEMO wall challenge,» *Nucl. Fusion*, vol. 57, n. 4, 9 feb 2017.

[6] R. Wenninger, F. Arbeiter, J. Aubert, L. Aho-Mantila, R. Albanese, R. Ambrosino, C. Angioni, J.-F. Artaud, M. Bernert, E. Fable, A. Fasoli, G. Federici, J. Garcia, G. Giruzzi, F. Jenko, P. Maget, M. Mattei, F. Maviglia, E. Poli, G. Ramogida, C. Reux, M. Schneider, B. Sieglin, F. Villone, M. Wischmeier and H. Zohm, "Advances in the physics basis for the European DEMO design," *Nuclear Fusion*, vol. 55, p. 063003, 2015.

[7] G. Federici, C. H. Skinner, J. N. Brooks, J. P. Coad, C. Grisola, A. A. Haasz, Philipps, V. Philipps , C. S. Pitcher, J. Roth, W. R. Wampler e D. G. Whyte, «Plasma-material interactions in current tokamaks and their implications for next step fusion reactors,» *Nucl. Fusion*, vol. 41, n. 12, pp. 1967-2137, dec 2001.

[8] M. Moscheni, M. Carr, S. Dulla, F. Maviglia, A. Meakins, G. F. Nallo, F. Subba and R. Zanino, "Radiative Heat Load Distribution on the EU-DEMO First Wall Due to Mitigated Disruptions," *Nuclear Materials and Energy, DOI: https://doi.org/10.1016/j.nme.2020.100824*, 2020.

[9] N. Commaux, D. Skiraki, L. R. Baylor, E. M. Hollmann, N. W. Eidietis , C. J. Lasnier, R. A. Moyer, T. C. Jernigan, S. J. Meitner, S. K. Combs and C. R. Foust, "First demonstration of rapid shutdown using neon shattered pellet injection for thermal quench mitigation on DIII-D," *Nuclear Fusion*, vol. 56.4, p. 46007, 2016.

[10] R. Sweeney, A. J. Creely, J. Doody, T. Fulop, D. T. Garnier, R. Granetz, M. Greenwald, L. Hesslow, J. Irby, V. A. Izzo, R. J. La Haye, N. C. Logan, K. Montes, C. Paz-Soldan, C. Rea, R. A. Tinguely, O. Vallhagen and J. Zhu, "MHD stability and disruptions in the SPARC tokamak," *J. Plasma Physics*, vol. 86, p. 865860507, 2020.

[11] M. Carr and A. Meakins, *cherab/core: Release v1.1.0*, Zenodo, 2019.

[12] M. Carr, A. Meakins, A. Baciero, M. Bernert, A. Callarelli, A. Field, C. Giroud, J. Harrison, N. Hawkes, S. Henderson and B. Lipschultz, "Towards Integrated Data Analisys of Divertor Diagnostics with Ray-Tracing," *44th EPS Conference on Plasma Physics*, 2017.

[13] M. Brank, R. Pitts, G. Simič, P. Lamalle, M. Kocan, F. Köchl, Y. Gribov, V. Polli and L. Kos, "Assessment of plasma power deposition on the ITER ICRH antennas," *Nuclear Materials and Energy*, vol. 27, p. 101021, 2021.

[14] R. Raman, R. Sweeney, R. A. Moyer, N. W. Eidietis, D. Shiraki, J. L. Herfindal, J. Sachdev, E. M. Hollmann, S. C. Jardin, L. R. Baylor, R. Wilcox, T. Carlstrom, T. Osborne, D. Eldon, J. E. Menard, R. Lunsford and B. Grierson, "Shattered pellet penetration in low and high energy plasmas on DIII-D," *Nuclear Fusion*, vol. 60, pp. 036014 - 15pp, 2020.

[15] F. Maviglia, C. Bachmann, G. Federici, T. Franke, M. Siccinio, R. Albanese, R. Ambrosino, R. Bonifetto, G. Calabrò, R. De Luca, E. Fable, P. Fanelli, A. Fanni, M. Firdaouss, J. Gerardin, R. Lombroni, M. Moscheni, F. Palermo, G. Pautasso, S. Pestchanyi, R. Giuseppe, M. L. Richiusa, G. Sias, F. Subba, F. Villone and Z. Vizvary, "Integrated strategy of limiter design for EU-DEMO first wall protection from plasma transients," *submitted to Fusion Engineering and Design*, 2020.

[16] F. Maviglia, C. Bachmann, G. Federici, T. Franke, M. Siccinio, C. Vorpahl, R. Albanese, R. Ambrosino, E. Fable, M. Firdaouss, J. Gerardin, V. P. Loschiavo, M. Mattei, F. Palermo, M. L. Richiusa, F. Villone and Z. Vizvary, "Impact of plasma thermal transients on the design of the EU DEMO first wall protection," *Fusion Engineering and Design*, vol. 158, p. 111713, 2020.

[17] M. Moscheni, "Modeling the radiative power load on the EU-DEMO PFCs during a mitigated plasma disruption," M.Sc. Thesis, Politecnico di Milano, 29 April 2020. [Online]. Available: https://www.politesi.polimi.it/handle/10589/153030. [Accessed 2020].

Formatted: Italian (Italy)

Formatted: English (United States)

Formatted: English (United States)

[18] T. Franke, M. Q. Tran and P. Spaeh, *Private Communication,* 2020.

[19] T. Franke, G. Aiello, K. Avramidis, C. Bachmann, B. Baiocchi, C. Baylard, A. Bruschi, D. Chauvin, A. Cufar, R. Chavan, C. Gliss, F. Fanale, L. Figini, G. Gantenbein, S. Garavaglia, G. Granucci, J. Jelonnek, G. Suárez López, A. Moro, M. Moscheni, N. Rispoli, M. Siccinio, P. Spaeh, D. Strauss, F. Subba, I. Tigelis, M. Tran, C. Tsironis, C. Wu and H. Zohm, "Integration concept of an Electron Cyclotron System in DEMO," *Fusion Engineering and Design,* vol. 168, p. 112653, 2021.

[20] E. Hollmann, P. Aleynikov, T. Fülöp, D. Humphreys, V. Izzo, M. Lehnen, V. Lukash, G. Papp, G. Pautasso, F. Saint-Laurent and J. Snipes, "Status of research toward the ITER disruption mitigation system," *Physics of Plasmas,* vol. 22, 2015.

[21] R. Muscia, "Symmetry of Magnetostatic Fields Generated by Toroidal Helicoidal Magnets," *IEEE Transactions on Magnetics,* vol. 51, no. 10, pp. 1-14, 2015.

[22] J. Hobirk, M. Bernert, P. Buratti, C. Challis, I. Coffey, P. Drewelow, E. Joffrin, J. Mailloux, I. Nunes, G. Pucella, T. Putterich, P. de Vries e JET contributors, «Analysis of plasma termination in the JET hybrid scenario,» *Nuclear Fusion,* vol. 58, n. 7, p. 076027, 2018.

[23] E. Hollmann, D. Gray, D. Whyte, A. Pigarov, S. Krasheninnikov, J. Boedo and D. Humphreys, "Radiated power measurement during the thermal quench phase of a density limit disruption," *Physics of Plasmas,* vol. 10, p. 2863, 2003.

[24] G. V. Pereverzev and P. N. Yushmanov, "ASTRA - Automated System for TRansport Analysis," Max-Planck-Institut Für Plasmaphysik, 2002.

[25] F. Subba, D. P. Coster, A. N. Escat Juanes, E. Fable, R. Wenninger and R. Zanino, "Analysis of Highly Radiative Scenarios for the EU-DEMO Divertor Target Pretection," *Contributions to Plasma Physics,* vol. 58, pp. 758-764, 2018.

[26] M. Carr and A. Meakins, *Private Communication,* 2019.

[27] R. J. Moffat, "Describing the uncertainties in experimental results," *Experimental Thermal and Fluid Science,* vol. 1, no. 1, pp. 3-17, 1988.

[28] A. Meakins e M. Carr, *raysect/source: Release 0.5.5,* Zenodo, 2019.

[29] M. Moscheni and G. F. Nallo, *Parametric Study of the Radiative Load Distribution on the EU-DEMO First Wall Due to SPI-Mitigated Disruptions and in Steady-State (dataset) (Version 1.0.0) [Data set],* Presented at the 31st Symposium on Fusion Technology (SOFT2020), Virtual edition: Zenodo. http://doi.org/10.5281/zenodo.5094247.

[30] A. Huber, G. Arnoux, M. N. A. Beurskens, S. A. Bozhenkov, S. Brezinsek, T. Eich, C. Fuchs, W. Fundamenski, S. Jachmich, U. Kruezi, M. Lehnen , A. Loarte, G. F. Matthews, P. Mertens, P. D. Morgan, V. Philipps, R. A. Pitts, V. Riccardo, U. Samm, B. Schweer, G. Sergienko, M. Stamp and JET EFDA Contributors, "Radiation loads onto plasma-facing components of JET during transient events – Experimental results and implications for ITER," *Journal of Nuclear Materials,* vol. 415, no. 1, pp. S821-S827, 2011.

[31] G. M. Olynyk, *Radiation Asymmetry and MHD Activity in Rapid Shutdowns on Alcator C-Mod,* Department of Nuclear Science and Engineering, MIT, 2013. Available at: https://dspace.mit.edu/bitstream/handle/1721.1/86421/878536832-MIT.pdf;sequence=2.

[32] F. P. Incropera, Introduction to Heat Transfer, Hoboken, NJ: John Wiley & Sons, 2011, pp. 310-315.

[33] J. Linke, J. Du, T. Loewenhoff, G. Pintsuk, B. Spilker, I. Steudel and M. Wirtz, "Challenges for plasma-facing components in nuclear fusion," *Matter and Radiation at Extremes,* vol. 4, no. 11, p. 056201, 5 2019.

[34] J. H. You, E. Visca, C. Bachmann, T. Barrett, F. Crescenzi, M. Fursdon, H. Greuner, D. Guilhem, P. Languille, M. Li, S. McIntosh, A. V. Muller, J. Reiser, M. Richou and M. Rieth, "European DEMO divertor target: Operational requirements and material-design interface," *Nuclear Materials and Energy,* vol. 9, pp. 171-176, 2016.

[35] P. Lang, F. Cismondi, C. Day, E. Fable, A. Frattolillo, C. Gliss, F. Janky, B. Pégourié and B. Ploeckl, "Optimizing the EU-DEMO pellet fuelling scheme," *Fusion Engineering and Design,* vol. 156, p. 111591, 2020\.